

Arm retraction dynamics in dense polymer brushes

M. Lang, M. Werner, R. Dockhorn, and T. Kreer

Large scale Monte Carlo simulations of dense layers of grafted polymer chains in good solvent conditions are used to explore the relaxation of a polymer brush. Monomer displacements are analyzed for the directions parallel and perpendicular to the grafting plane. Auto-correlation functions of individual segments or chain sections are monitored as function of time. We demonstrate that the terminal relaxation time τ of grafted layers well in the brush regime grows exponentially with degree of polymerization N of the chains, $\tau \propto N^3 \exp(N/N_e)$, with N_e the entanglement degree of polymerization in the brush. One specific feature of entangled polymer brushes is that the late time relaxation of the perpendicular component coincides for all segments. We use this observation to extract the terminal relaxation time of an entangled brush.

I. INTRODUCTION

Polymer brushes are layers of polymer chains grafted densely onto a surface. These brushes can be used in various applications ranging from drug delivery [1], colloid stabilization [2, 3], and lubrication [4–8], to switchable amphiphilic surfaces [9]. In recent years, brushes made of more complex architectures like stars [10], cyclic polymers [11], dendrimers [12] along with cross-linked brushes [13, 14], or systems containing nano-inclusions [15, 16] were analyzed.

The relaxation dynamics of polymer brushes is of great importance for understanding the polymer-brush lubrication [7, 17], which itself is relevant for medical implants [6, 18, 19], drug delivery [20], microfluidic devices [21, 22], and so forth. Also, the ultra-low friction of human joints motivated work on out-of-equilibrium conformations and dynamics of polymer brush bi-layers [15, 23–25] and kinetic barriers have been identified as limiting factors for the formation of nano-aggregates using bridging of surfaces via polymer brushes [26] to provide just some examples of current research.

With these increasingly diverse research topics and applications, a general understanding of the most fundamental case, a densely grafted layer of monodisperse linear chains, is highly in demand. Even though a large number of self-consistent field approaches have been published previously, see for instance Refs. [27–31], a self-consistent model that leads to the same free energy as scaling models [32, 33] was developed only recently [34]. Concerning the relaxation dynamics, simulation data and theoretical models still are controversial as briefly summarized below.

For a polymer brush, it is generally assumed that the grafting density σ defines the correlation length,

$$\xi \approx \sigma^{-1/2}, \quad (\text{I.1})$$

at which neighboring strands start to interact [32, 33]. This length is spanned in average by a short strands of

$$g \approx (\xi/b)^{1/\nu} \approx \sigma^{-1/(2\nu)} b^{-1/\nu} \quad (\text{I.2})$$

Kuhn segments. Here, b is the root mean square size of a Kuhn segment and $\nu \approx 0.588$ is the Flory exponent describing polymer conformations in good solvent [35, 36], while $\nu = 1/2$ for θ solvents. In the “brush regime”, the overlap of the chains leads to a swelling of polymers

made of N Kuhn segments to a layer of thickness [32, 33]

$$H \approx \xi N/g \approx N \sigma^{(1-\nu)/(2\nu)} b^{1/\nu}. \quad (\text{I.3})$$

For friction dominated dynamics, the relaxation time of a correlation volume, τ_ξ , can be estimated [37] as

$$\tau_\xi \approx \tau_0 g^{2\nu+1} \approx \tau_0 \sigma^{-(2\nu+1)/(2\nu)} b^{-(2\nu+1)/\nu} \quad (\text{I.4})$$

using the monomer relaxation time, τ_0 . For non-entangled brushes, the terminal relaxation time was first estimated in Ref. [38] using a dumbbell model. The stretched chain conformations in direction perpendicular to the grafting plane lead to an extended relaxation time

$$\tau_{\perp,d} \propto \tau_\xi (N/g)^3 \propto \sigma^{(1-\nu)/\nu} b^{-(2-2\nu)/\nu} N^3, \quad (\text{I.5})$$

as compared to the parallel directions, where the relaxation time scales as

$$\tau_{\parallel,d} \propto \tau_\xi (N/g)^2 \propto \sigma^{-(2\nu-1)/(2\nu)} b^{-(2\nu-1)/\nu} N^2. \quad (\text{I.6})$$

In good solvent, both results are approximately $\propto \sigma^{2/3}$ and $\sigma^{-1/6}$ respectively, while these results become $\propto \sigma^1$ and $\propto \sigma^0$ for θ solvents. Note that a similar result would be obtained using the Rouse model as basis for computation.

Hydrodynamics up to the scale of a blob renormalizes the blob relaxation time $\tau_\xi \approx \tau_0 g^{3\nu}$ for good solvents as introduced first in Ref. [39] for a polymer brush. This leads to relaxation times for this model with

$$\tau_{\perp,h} \propto \sigma^{3(1-\nu)/(2\nu)} N^3 \approx \sigma^{1.05} N^3 \quad (\text{I.7})$$

in perpendicular direction and

$$\tau_{\parallel,h} \propto \sigma^{(2-3\nu)/(2\nu)} N^2 \approx \sigma^{0.20} N^2 \quad (\text{I.8})$$

in parallel direction (θ -solvent: $\propto \sigma^{3/2}$ and $\propto \sigma^{1/2}$, respectively). The difference to the friction dominated case above lies only in the modified scaling as function of the grafting density σ . Note also that the stretching field of the brush allows in both cases for extra large dynamic fluctuations of the chain extensions $\propto N$ in perpendicular direction [38]. Non-entangled chains in a brush, therefore, are “swollen” coils and relax in self-similar manner on all subscales in a first approximation (up to small corrections with respect to the particular shape of the brush potential).

A qualitatively different result is obtained for entangled polymer brushes. Here, the terminal relaxation time is expected [40] to increase exponentially as function of the number of effective monomers (here: N/g correlation volumes) for large N ,

$$\tau \propto (N/g)^3 \exp(N/g), \quad (\text{I.9})$$

since terminal relaxation is governed by the arm retraction dynamics of the grafted polymers similar to the relaxation of branched polymers.

Let us number the entangled sections starting from the grafting point with a variable s up to $s_{max} = N/N_e$ at the free end. Here, N_e is the entanglement degree of polymerization. For arm retraction dynamics, atypically large tube length fluctuations are required to release entanglements of sections $s \lesssim s_{max} - (N/N_e)^{1/2}$. Usually, this is modeled as a thermally activated process in an effective potential that is approximated by a parabola [37]

$$U(s) \approx \frac{\gamma kT}{2} \frac{(s_{max} - s)^2 N_e}{N}, \quad (\text{I.10})$$

where γ is an effective dimensionless spring constant of order unity, k the Boltzmann constant and T the absolute temperature. Note that because of this effective potential we have to consider now “stretched” chains with reduced dynamic fluctuations instead of “swollen” ones. This approximation leads to an exponential decrease $\propto \exp\left(-\frac{\gamma(s_{max}-s)^2 N_e}{2N}\right)$ of the probability for finding tube lengths that are reduced to s sections. As consequence, the time it takes to release entanglement number s by retraction grows exponentially for decreasing s

$$t(s) \propto \tau_a \exp\left(\gamma(s_{max} - s)^2 N_e / (2N)\right). \quad (\text{I.11})$$

τ_a is the “attempt time” of retractive motion and related to the Rouse time of the polymer in the particular environment. Due to the exponential increase in relaxation times, the number $(s_{max} - s)$ of entanglements released per chain is roughly the same for all chains at time t and grows logarithmically at large times:

$$s_{max} - s(t) \propto (2N/(\gamma N_e))^{1/2} (\ln(t/\tau_a))^{1/2}. \quad (\text{I.12})$$

O’Connor and McLeish used arm retraction dynamics to study the adhesion of a polymer network on a dry brush [41, 42]. They argue that for a brush penetrating a network, the brush self-consistent potential should enter only as a small (logarithmic) correction to τ_a ,

while the exponential increase with the degree of polymerization N is not modified. We expect a similar behaviour for monodisperse brushes in good solvent. However, the different Rouse times in parallel and perpendicular direction, see equations (I.5) and (I.6), lead to a shorter attempt time τ_a for retractive motion in parallel directions. This could drive disentanglement of the chains in parallel directions without the need for retractive motions in perpendicular direction.

It is also instructive to mention the relaxation of a single chain in an array of straight rods that are grafted perpendicular to a surface as a limiting case of relaxation in anisotropic entanglements. Here, the retraction dynamics in directions parallel to the grafting plane becomes decoupled from the Rouse relaxation in perpendicular direction on time scales beyond the entanglement time. A similar behavior as for this limiting case might be visible in an entangled polymer brush at intermediate times between the entanglement relaxation times in parallel and perpendicular direction, $\tau_{e\parallel} < t < \tau_{e\perp}$, if $\tau_{e\perp}/\tau_{e\parallel} \approx N_e/g$ is sufficiently large. Note that $\tau_{e\parallel}$ and $\tau_{e\perp}$ are readily obtained from inserting N_e instead of N into equations (I.5) and (I.6) or, if hydrodynamics is important, equations (I.7) and (I.8).

Finally, we have to mention that entangled brushes refer to a case, where the chains inside the confining tubes are largely “over-stretched”. This point follows from $N_e > g$ in a semi-dilute solution of flexible polymers [37] and the fact that the correlation blob size equals the tension blob size in a brush [33]. Thus, the tension blobs are smaller than the length scale that is typically associated with an entanglement (“tube diameter”). This leads to entangled sections of size $a_{\parallel} \approx \xi(N_e/g)^{1/2}$ and $a_{\perp} \approx \xi(N_e/g)$ that consist of a small series [43] of essentially pairwise chain contacts that are pulled taught within volumes of order ξ^3 . This is quite different to entanglements in a melt with a lateral tube confinement of order $a \approx bN_e^{1/2}$. In consequence, small chain sections of extra g monomers that can fold a distance ξ away from the primitive path of this “over-stretched” tube require kT on energy and, thus, become exponentially rare. Hence, we expect to determine the blob size ξ instead of the size of an entangled section when analyzing the lateral confinement along the tube in the vicinity of the grafting plane.

The exponentially increasing relaxation times mentioned above were successfully tested in several experiments [46–49] on the adhesion of bulk polymer materials like networks or entangled melts on a polymer brush. Previous simulation works [50–57], however, confirm

mainly the estimates for the non-entangled case, see Table I. Only the authors of one work [53] suggest an exponential increase of the relaxation time already for a rather small number of N/g . In a simulation of two brushes sliding on top of each other, also an almost logarithmic relaxation of the end-to-end vector of the chains was found for rather small $N = 60$ and a grafting density only about twice as high as the overlap grafting density [58]. More recent work [57] covering a much larger N/g observes an effective relaxation time $\propto N^{3.7}$ in disagreement to previous theoretical works [38–42, 68]. Quite unexpectedly, the largest relaxation times were found near the middle of the chains, where the relaxation in parallel directions was slower than in perpendicular direction. A qualitatively similar result was obtained in a second study for spherical brushes [59].

We attempt to resolve this puzzle by a comparison of different observables (monomer mean square displacements and auto-correlation functions) that are analyzed such that the differences concerning entangled and non-entangled brushes or concerning other points raised in the introduction stand out. In addition, we test the concepts introduced above and discuss how to correctly determine the terminal relaxation time of an entangled polymer brush.

II. COMPUTER SIMULATIONS

Since we want to understand the universal behavior of brushes formed from flexible chains, we use the Bond Fluctuation Model (BFM) as introduced by Carmesin and Kremer [60] and extended to three dimensions by Deutsch and Binder [61]. In this model, each monomer is represented by a cube of eight lattice positions on a simple cubic lattice. The monomers of a chain are connected by bond vectors out of a particular vector set. The motion of the monomers occurs via random displacements by one lattice unit along a lattice axis, where those moves are rejected for which the new particle position leads to overlap of monomers or to bond vectors not contained in the set. Solvent is treated implicitly in the a-thermal limit. Because of the neglect of momentum and solvent, no hydrodynamic effects are modeled and dynamics is friction dominated. In order to collect data over an extremely long time interval, we use a GPU implementation of the BFM [62], which leads to equivalent data concerning the dynamics as compared to the original implementations at a slightly enlarged effective excluded volume.

Method	System	direction	analysis	N	σ	τ	Ref.
MD	a-thermal	O	EAT	$10 \leq 100$	$0.03 \leq 0.1$	$\propto N^{2.5 \pm 0.1} \sigma^{0.5}$	[50]
BFM	a-thermal	\perp	CAT	$10 \leq 60$	$0.025 \leq 0.2$	$\propto N^{3.0 \pm 0.01} \sigma^{0.83 \pm 0.08}$	[51]
BFM	Θ -solvent	\perp	CAT	$20 \leq 50$	$0.05 \leq 0.125$	$\propto N^3 \sigma^{1.6}$	[52]
LMC	a-thermal	O	DS	$50 \leq 100$	$0.02 \leq 0.08$	$\propto N^2 \sigma^{-1/6}$	[53]
LMC	a-thermal	\perp	DS	$50 \leq 100$	$0.02 \leq 0.08$	$\propto N^3 \sigma^{2/3}$	[53]
LMC	a-thermal	\perp & O	DS	50	0.12	exponential?	[53]
BFM	a-thermal	\parallel	CAT	$20 \leq 60$	$0.05 \leq 0.1$	$\propto N^2 \sigma^{-1/6}$	[54]
BFM	a-thermal	\perp	CAT	$10 \leq 80$	$0.025 \leq 0.2$	$\propto N^3 \sigma^{2/3}$	[54]
MD	brush in melt	O	EAT, RAT	$50 \leq 200$	$0.01 \leq 0.41$	$\propto N^3 \sigma$	[55]
MD	a-thermal	\parallel	MSD	$64 \leq 128$	$0.013 \leq 0.492$	$\propto N^2 \sigma^{-1/6}$	[56]
MD	a-thermal	\perp	MSD	$64 \leq 128$	$0.013 \leq 0.492$	$\propto N^3$	[56]
MC+MD	a-thermal	\perp	MSD, RAT	$16 \leq 64$	0.125	$\propto N^3$	[57]
MD	a-thermal	\parallel & \perp	MSD, RAT	$64 \leq 512$	0.125	$\propto N^{3.7}$	[57]
BFM	a-thermal	\parallel, \perp & O	MSD, TTAA	$16 \leq 128$	$1/16 \leq 1/4$	$\propto N^3 \exp(N)$	this work

Table I. Terminal relaxation times, as determined by computer simulations. We compare results from molecular dynamics simulations (MD), the Bond Fluctuation Method (BFM), off-lattice Monte Carlo (MC), and lattice Monte Carlo simulations (LMC). All “systems” concern homopolymer brushes of monodisperse chain lengths under different solvent conditions. The analyzed directions are either isotropic (“O”), perpendicular to the grafting plane (“ \perp ”), or parallel to the grafting plane (“ \parallel ”). EAT, CAT, RAT, and DS are the end-to-end vector auto-correlation time, the directional component auto-correlation time, radius of gyration (or its spacial components) auto-correlation time, or dynamic scattering, respectively. TTAA denotes the terminal time auto-correlation analysis as introduced in section III B. For EAT, CAT, RAT, and DS, the relaxation time was always defined by the decay of the function to $1/e$. MSD refers to an analysis of the mean square displacements. The data range for the degree of polymerization, N , and the grafting density, σ , is indicated along with the suggested scaling of the terminal relaxation time, τ .

Sample	#1	#2	#3	#4	#5	#6	#7	#8
N	16	32	64	64	64	128	128	128
σ	1/4	1/4	1/4	"1/9"	1/16	1/4	"1/9"	1/16
M	1024	1024	1024	1764	4096	1024	882	1024
τ [MCS]	$2.5 \cdot 10^5$	$2.4 \cdot 10^6$	$4.9 \cdot 10^7$	$1.0 \cdot 10^7$	$5.3 \cdot 10^6$	$8.6 \cdot 10^9$	$4.9 \cdot 10^8$	$1.0 \cdot 10^8$
t_{tot} [MCS]	$1.2 \cdot 10^7$	$7.7 \cdot 10^9$	$2.2 \cdot 10^{10}$	$5 \cdot 10^8$	$2.9 \cdot 10^9$	$2.7 \cdot 10^{10}$	$9.9 \cdot 10^9$	$7.6 \cdot 10^9$

Table II. Simulation parameters for degree of polymerization, N , grafting density, σ , and number of grafted chains per sample, M . Note that σ is normalized to the maximum possible grafting density in the BFM model, which is 0.25 in square lattice units. The exact grafting density for samples 4 and 7 is 441/4096 (we use "1/9" to simplify notation in Tables and Figures but use the exact value for computation). The terminal relaxation time τ is determined using the perpendicular component of the position vector auto-correlation function as described in section III B. The last row indicates the total duration t_{tot} of the simulation runs.

For the present study, we focus on brushes at rather large grafting densities and chain lengths in order to explore the dynamics of entangled brushes. Periodic boundary conditions were applied in the directions parallel to the grafting plane. The perpendicular dimension of the simulation box was chosen sufficiently large to avoid confinement by the box size.

Initial chain conformations were relaxed prior to analysis for several terminal relaxation times τ , which was determined as described below in section III. Production runs spanned at least 20 relaxation times. The only exception is sample #6, for which only 3 relaxation times could be realized, see Table II. Since no qualitative variation of the results of sample #6 (except of a clearly larger scatter of the data) was detected, we consider all samples as sufficiently equilibrated for analysis.

III. RESULTS

In this section, we summarize only the results for the dynamics of polymer brushes, since the data on chain conformations (with extra data in the low σ limit) were published previously in Ref. [34]. Let n denote the number of the monomers along a chain as counted from the grafting point. $\mathbf{R}_n(t)$ is the position vector of monomer n at time t with respect

to the grafting point of the chain. We consider long chains of N monomers in the brush regime with $N \gg g$, where g is the number of monomers per concentration blob. b is the ensemble average root mean square length of a bond between any two connected monomers. Ensemble averages over all chains are denoted by angular brackets $\langle \dots \rangle$. The statistics of all dynamic quantities is improved by averaging over a large set of different starting times. Local dynamics are analyzed by means of the normalized bond auto-correlation function

$$b_c(n, \Delta t) = \frac{\langle \mathbf{b}_n(t) - \langle \mathbf{b}_n \rangle, \mathbf{b}_n(t + \Delta t) - \langle \mathbf{b}_n \rangle \rangle}{\langle (\mathbf{b}_n(t) - \langle \mathbf{b}_n \rangle)^2 \rangle} \quad (\text{III.1})$$

for oriented chains, whereas relaxation from the free end is analyzed by using the auto-correlation function

$$a_c(n, \Delta t) = \frac{\langle \mathbf{R}_n(t) - \langle \mathbf{R}_n \rangle, \mathbf{R}_n(t + \Delta t) - \langle \mathbf{R}_n \rangle \rangle}{\langle (\mathbf{R}_n(t) - \langle \mathbf{R}_n \rangle)^2 \rangle}, \quad (\text{III.2})$$

of the position vector $\mathbf{R}_n(t)$. Here, b_n is the root mean square length of the bond vector $\mathbf{b}_n = \mathbf{R}_n - \mathbf{R}_{n-1}$ between monomers n and $n - 1$. \mathbf{R}_{n-1} is the zero vector for $n = 1$. The average vectors $\langle \mathbf{x}_n \rangle$, with $\mathbf{x} = \mathbf{R}, \mathbf{b}$ are required for proper normalization of the directional contributions perpendicular to the grafting plane. The time average vector components in parallel directions are assumed to be zero and the above expressions are equivalent to standard normalized vector auto-correlation functions in this case. As in the introduction, the directional contributions parallel and perpendicular to the grafting plane are denoted by the corresponding subscripts \parallel and \perp . Directional mean square displacements (or monomer relaxation times, auto-correlation times, etc ...) are determined using the directional components of vectors \mathbf{b}_n or \mathbf{R}_n , respectively.

A. Monomer mean square displacements

The mean square displacement of monomer n can be written as a function of the time interval Δt for an arbitrary starting time t

$$\langle [d_n(\Delta t)]^2 \rangle = \langle [\mathbf{R}_n(t + \Delta t) - \mathbf{R}_n(t)]^2 \rangle. \quad (\text{III.3})$$

In Figures III.1 and III.2, we show an example for the monomer mean square displacements as function of Δt for perpendicular and parallel directions separately. For comparison

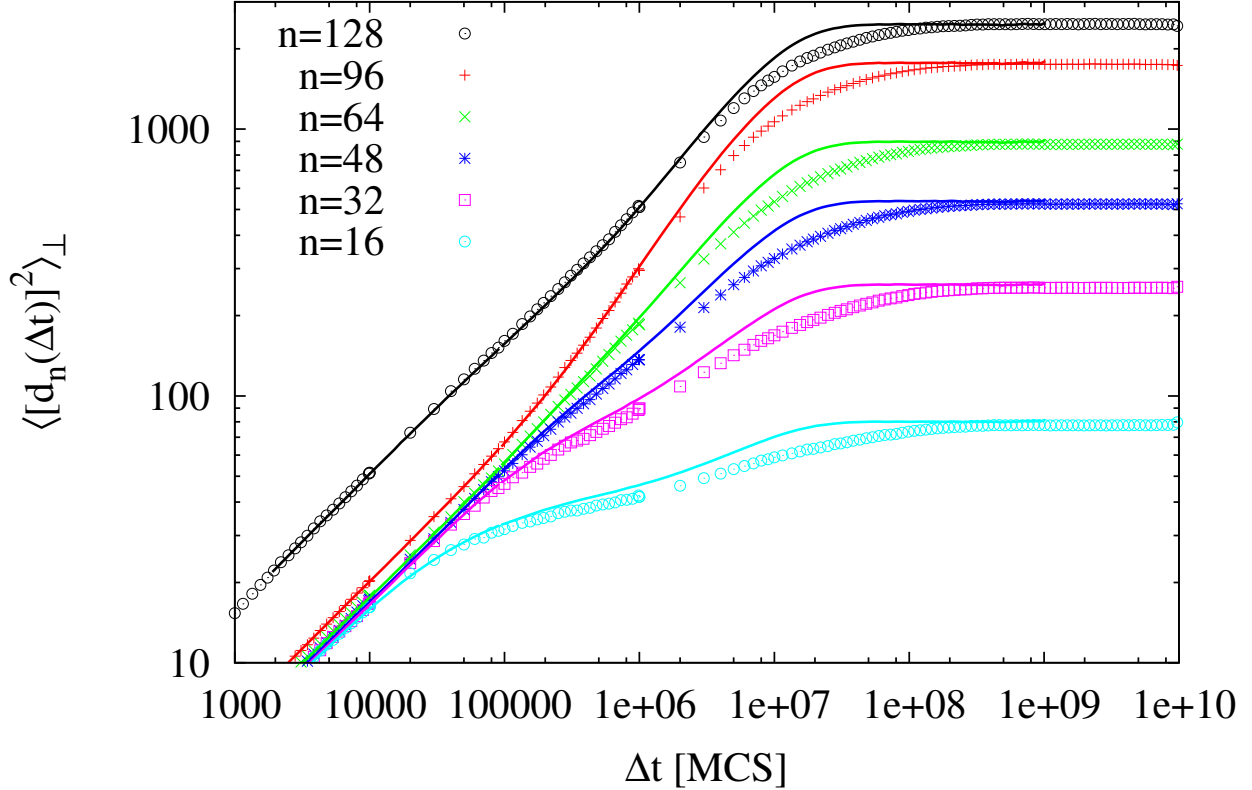


Figure III.1. Monomer mean square displacements in perpendicular direction, $\langle [d_n(\Delta t)]^2 \rangle_{\perp}$, for different monomers n of sample #7 with $N = 128$ and $\sigma = 1/9$. The lines show the numerical solution of the Rouse model [57, 63] with mean square displacements $\propto t^{1/2}$ that was rescaled to match maximum displacements and local friction coefficients, see text for details.

with the numerical solution of a grafted Rouse chain of Refs. [57, 63], the theoretical lines were shifted for each n individually along the time axis to match the displacements near $\langle [d_n(\Delta t)]^2 \rangle_{\perp} \approx \xi^2$ and along the displacement axis to match the plateau at large Δt . These shifts compensate differences in the average friction coefficients and the different extensions of subsections of the chains as function of n .

In case of non-entangled brushes, we expect a good agreement between these theoretical lines and the data in *parallel* directions, while the agreement should be poor in *perpendicular* directions, since $\langle [d_n(\Delta t)]^2 \rangle_{\perp} \propto t^{2\nu/(1+2\nu)} \propto t^{2/3}$ for the self-similar relaxation of a swollen Rouse chain of size $R \approx bN^{\nu}$ with $\nu = 1$. For entangled brushes we expect qualitatively the opposite trend: poor agreement in parallel directions, since the monomers are confined

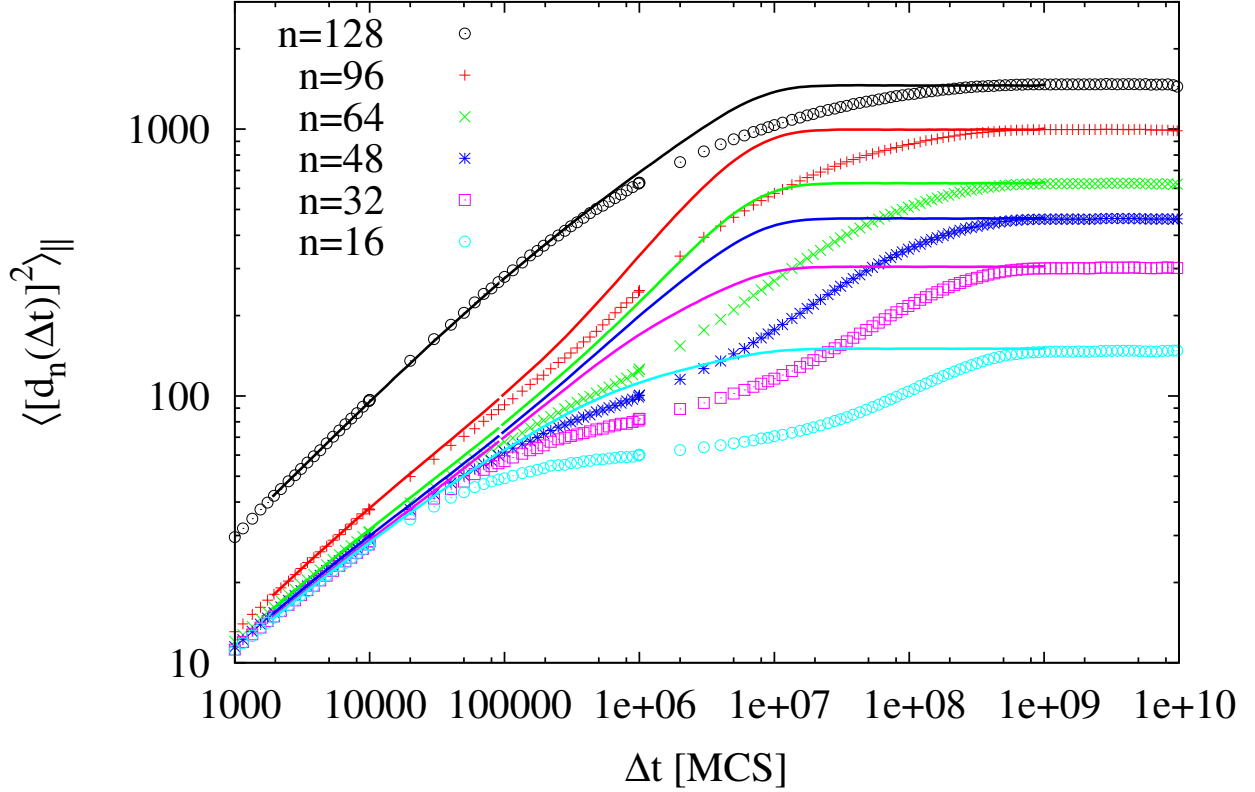


Figure III.2. Monomer mean square displacements parallel to the grafting plane, $\langle [d_n(\Delta t)]^2 \rangle_{\parallel}$, for different monomers n of sample #7.

inside the tube, while the data in perpendicular direction should follow Rouse dynamics up to the Rouse time of the chain, if the entanglements damp out the enlarged fluctuations in the perpendicular direction. The Rouse regime could be followed by a logarithmic regime, if the exponentially rare retractions of the chains contribute significantly to the mean square displacements.

The data of both Figures are a strong hint towards entangled dynamics. Since we observe no extended fluctuations in perpendicular directions, there are either only few entanglements per chain such that tube length fluctuations essentially dominate the perpendicular fluctuations or the exponentially rare retractions do not significantly contribute in perpendicular direction. Most characteristic for the data in parallel directions is the extended cross-over from initial mean square displacements (approximately $\propto t^{1/2}$) to a delayed equilibrium of mean square displacements and the two apparent relaxation steps of $\langle [d_n(\Delta t)]^2 \rangle_{\parallel}$ at small

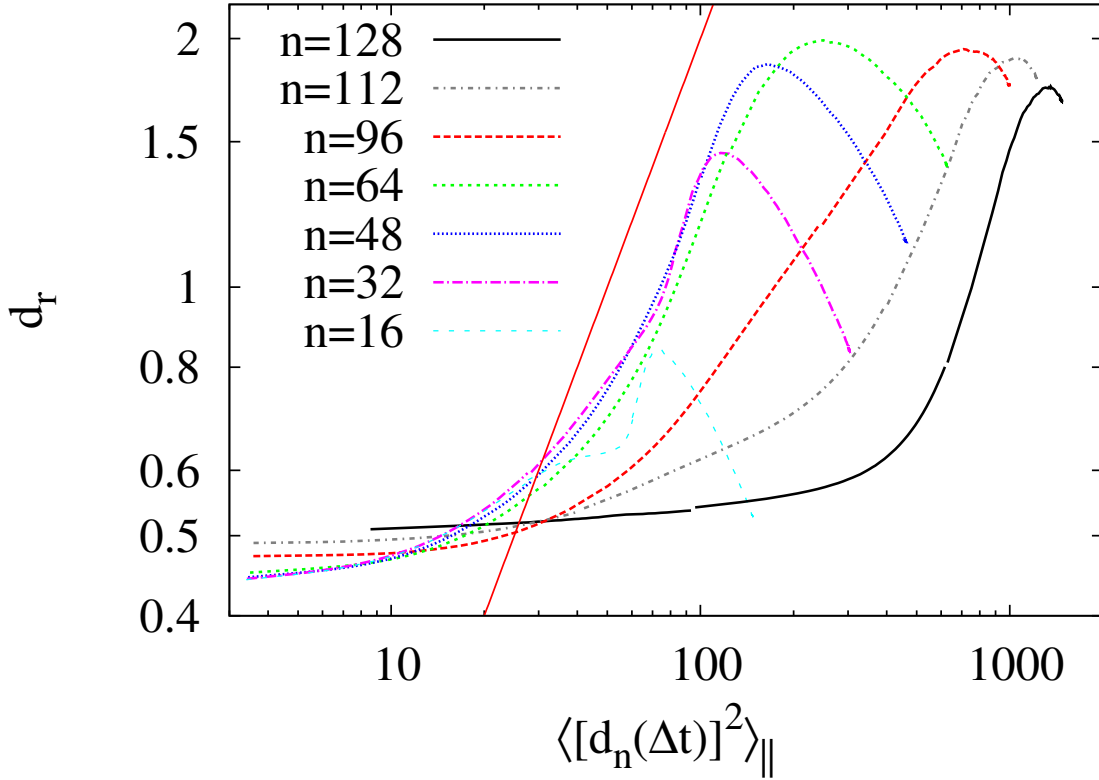


Figure III.3. Ratio d_r of the monomer mean square displacements in perpendicular and parallel directions (see Figures III.1 and III.2) as function of the displacement in parallel direction. The straight line indicates $d_r \propto \langle [d_n(\Delta t)]^2 \rangle_{\parallel}$.

n .

For a better qualitative understanding of the data, we plot the ratio

$$d_r \equiv \langle [d_n(\Delta t)]^2 \rangle_{\perp} / \langle [d_n(\Delta t)]^2 \rangle_{\parallel} \quad (\text{III.4})$$

as function of $\langle [d_n(\Delta t)]^2 \rangle_{\parallel}$ in Figure III.3. This compensates the effects of a different monomer mobility and allows for a more striking distinction [64] between the models discussed in the introduction.

All models [38–42, 68] start with an isotropic local motion of the monomers on a length scale below blob size. Thus, we expect constant displacement ratios of

$$d_r = 1/2 \quad (\text{III.5})$$

for small $\langle [d_n(\Delta t)]^2 \rangle_{\parallel} \lesssim \xi^2$ and $\tau < \tau_{\xi}$. Monomer diffusion becomes anisotropic for an anisotropically swollen Rouse chain beyond the blob size with $\langle [d_n(\Delta t)]^2 \rangle_{\perp} \propto t^{2/3}$, leading to

$$d_r \approx \frac{1}{2} \left\{ \langle [d_n(\Delta t)]^2 \rangle_{\parallel} / \xi^2 \right\}^{1/3} \quad (\text{III.6})$$

for $t < \tau_{\parallel,d}(n)$ or

$$\langle [d_n(\Delta t)]^2 \rangle_{\parallel} \lesssim \frac{\xi^2 n}{g}. \quad (\text{III.7})$$

For $\tau_{\parallel,d}(n) < t < \tau_{\perp,d}(n)$, only the mean square displacements in perpendicular directions grow up to

$$\langle [d_n(\Delta t)]^2 \rangle_{\perp} \approx \frac{\xi^2 n^2}{g^2}. \quad (\text{III.8})$$

Thus, we obtain three regimes for the non-entangled dynamics of polymers swollen in the stretching field of a brush: $d_r = \text{const.}$ followed by a power law with power 1/3 and an individual, sharp vertical increase of d_r for each n at the corresponding maximum mean square displacement in parallel directions.

In case of arm retraction [40], the initial regime, equation (III.5) is obtained up to $\langle [d_n(\Delta t)]^2 \rangle_{\parallel} \lesssim \xi^2$. For larger displacements, the motions of inner monomers are confined within an “over-stretched” tube of diameter ξ . This tube is similarly stretched as the chain conformations in the brush, and thus, performs a random walk in parallel directions, while it can be considered as a fully stretched array of entangled sections in perpendicular direction. This geometrical constraint leads to

$$d_r \propto \langle [d_n(\Delta t)]^2 \rangle_{\parallel} \quad (\text{III.9})$$

for $\xi^2 \lesssim \langle [d_n(\Delta t)]^2 \rangle_{\perp} \lesssim \xi^2 n^2 / (3g^2)$. Full exploration in parallel directions requires a sufficient number of full retractions, while these exponentially rare retractions contribute only little to the mean square displacements in perpendicular direction. Thus, the limiting $\langle [d_n(\Delta t)]^2 \rangle_{\parallel}$ at very large Δt should appear delayed as compared to the mean square displacements in perpendicular direction near to the limiting $\langle [d_n(\Delta t)]^2 \rangle_{\perp}$. Therefore, while $\langle [d_n(\Delta t)]^2 \rangle_{\perp}$ is roughly constant, $\langle [d_n(\Delta t)]^2 \rangle_{\parallel}$ remains growing, which implies a broad crossover from $d_r \propto \langle [d_n(\Delta t)]^2 \rangle_{\parallel}$ to a dependence

$$d_r \propto \langle [d_n(\Delta t)]^2 \rangle_{\parallel}^{-1} \quad (\text{III.10})$$

near maximum mean square displacements in parallel directions.

We show the ratio d_r for the mean square displacements of selected monomers of sample #7 in Figure III.3. All data show an initially constant $d_r \approx 1/2$ as expected for isotropic monomer motion. For essentially all inner monomers (small n), this regime is followed by a regime with $d_r \propto \langle [d_n(\Delta t)]^2 \rangle_{\parallel}$ until the data turn into $d_r \propto \langle [d_n(\Delta t)]^2 \rangle_{\parallel}^{-1}$ near the largest displacements. Thus, Figure III.3 demonstrates that the chains of this brush are clearly entangled.

The outermost monomers $n \approx 128$ are partially in agreement with the qualitative behavior predicted for an anisotropically swollen Rouse chain. The large correlation blob size near the free end monomer probably prevents the observation of the $1/3$ power law predicted above. A small downturn region is visible near the end, which indicates a marginal impact of entanglements. For $n < 128$, a gradual transition to the behavior of the entangled inner monomers is observed, see $n = 96, 112$ for examples.

For a quantitative test of our discussion above concerning tension blobs that are smaller than tube diameter, we extrapolate the data for small n with $d_r \propto \langle [d_n(\Delta t)]^2 \rangle_{\parallel}$ towards a level of $d_r = 1/2$. We find an intersection point at a mean square displacement of 37 ± 3 square lattice units for all $N/4 < n < N/2$, which is identical within the error bars with the average square distance between the grafting points, ξ^2 . Thus, the entanglements are pulled taught by the large tension along the chains and we can consider each polymer strand roughly as an independent obstacle where other chains have to wind around. With $2b^2/3 \approx 4.7$ for our simulation model in parallel directions, we estimate for the average number of monomers between two consecutive contacts (or the mean distance between slip-links - not to be confused with tube diameter [45]), N_p , that $N_p \approx 8$ for $\sigma \approx 1/9$ in sample #7. Note that the above extrapolation of d_r is the dynamic equivalent of determining blob size from polymer conformations. The good agreement of the intersection point with ξ^2 allows us to estimate the number of monomers per “dynamic blob” by setting $g = (\xi/b)^{1/\nu}$ without additional numerical coefficients. This relation is used below for a quantitative analysis of the relaxation times.

As bottom line of the above section we conclude that the relaxation in perpendicular and parallel directions must be coupled by confinement in a tube; at least we have no other explanation for the behavior of d_r in Figure III.3. The slow approach of the limiting

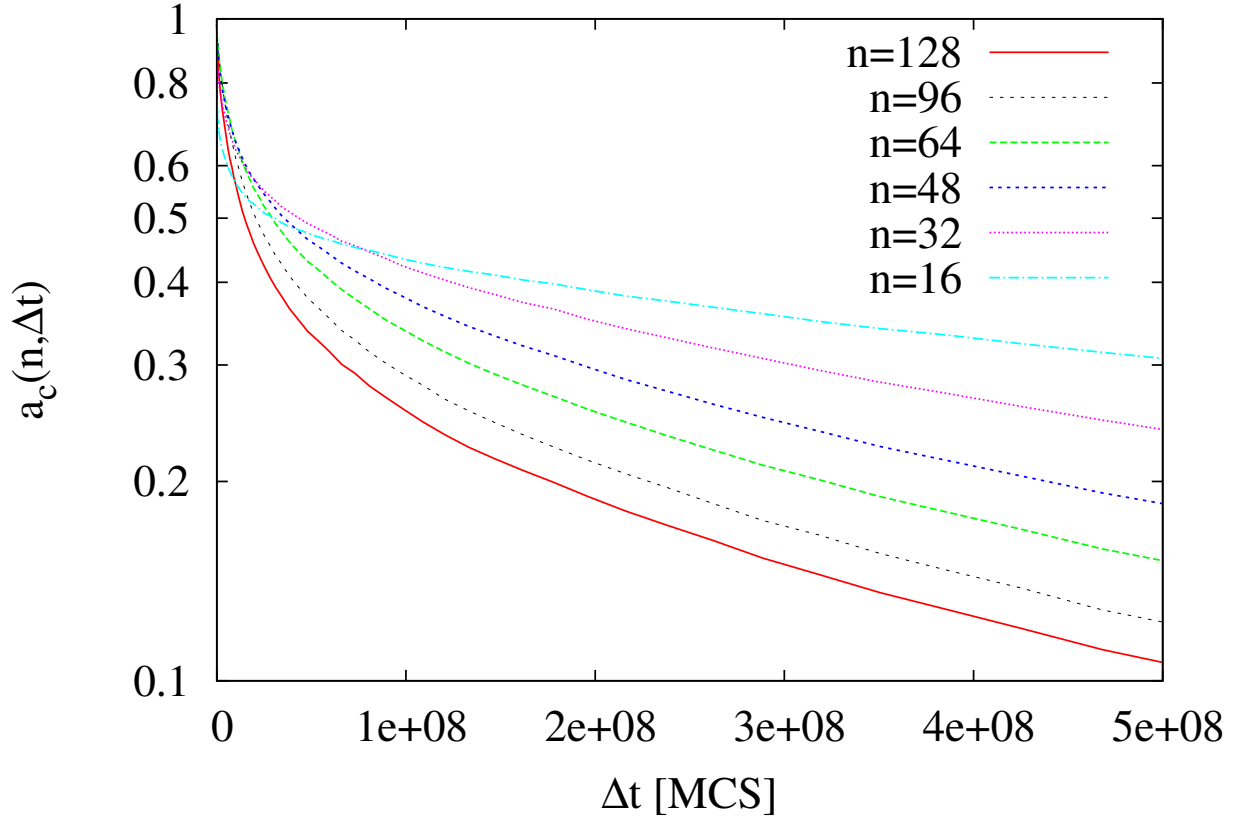


Figure III.4. Isotropic position vector auto-correlation function $a_c(n, \Delta t)$ for sample #6.

mean square displacements in Figure III.1 and III.2 makes it rather difficult to conclude on terminal relaxation times using mean square displacement data. In the following section, we discuss how to analyze the terminal relaxation time of a polymer brush using auto-correlation functions.

B. Position vector auto-correlation function and terminal relaxation times

The isotropic position vector auto-correlation function $a_c(n, \Delta t)$ given by equation (III.2) is plotted in Figure III.4 in the standard way (semi-log plot with linear time axis) for analyzing linear polymers. As expected from the previous section, there is no dominating single exponential decay as a function of time that can be used to identify a terminal relaxation. Note that such an approach also fails for the outermost monomers with largest n . Taking a decay to a fixed level of, for instance, $1/e$ as criterion for determining the relaxation time

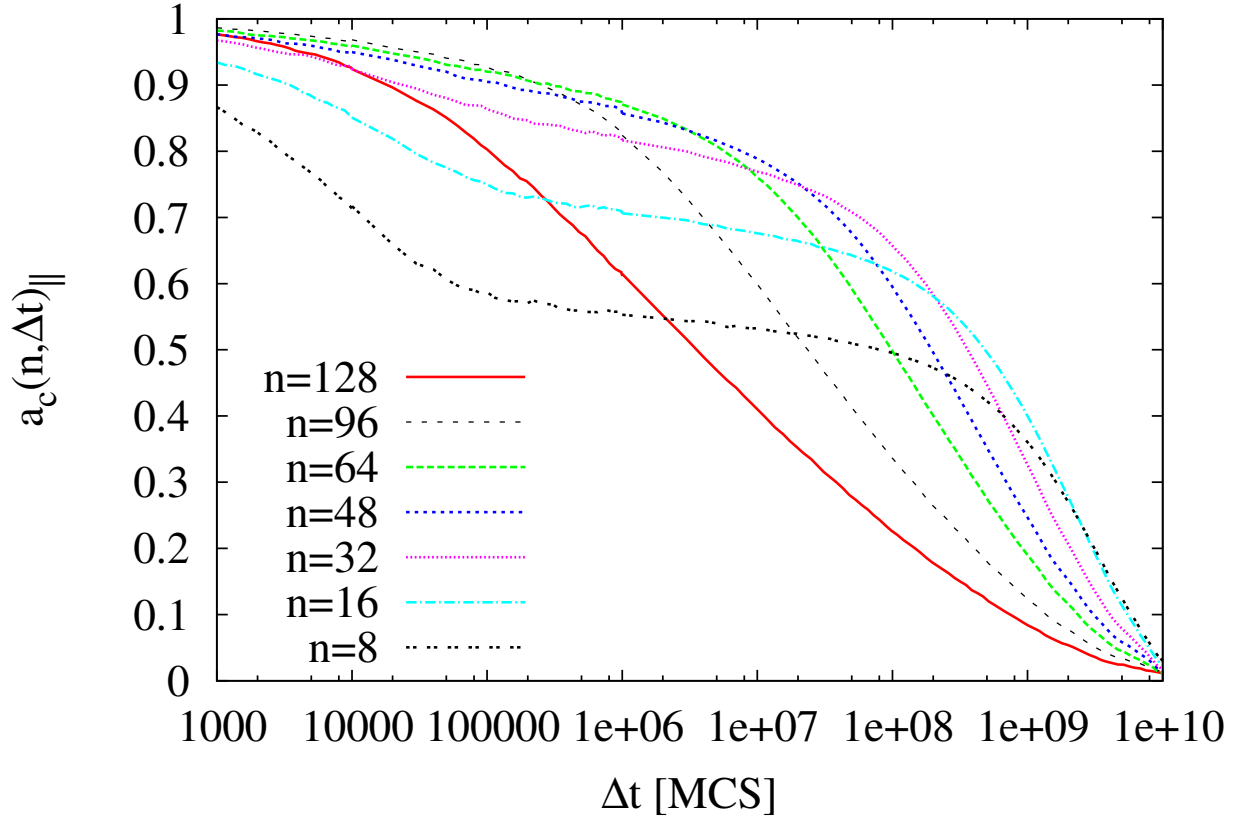


Figure III.5. Position vector auto-correlation function $a_c(n, \Delta t)_\parallel$ in parallel directions for sample #6.

(using EAT, CAT, RAT, or DS, see Table I) misses the increasingly slowed down relaxation at longer times, see Figure III.4.

Let us now discuss the directional components of the auto-correlation function in perpendicular and parallel directions separately (Figures III.5 and III.6) using a logarithmic time axis as suitable for understanding activated relaxation, see equation (I.12). Again, we observe clear qualitative differences between parallel and perpendicular directions. The data of the inner monomers (small n) of the parallel directions in Figure III.5 follow qualitatively the expectations of arm retraction models: after an initial quick Rouse-like decay, there is a logarithmic plateau that is stable for several decades in time until the innermost tube sections relax. The data at largest times show that terminal relaxation occurs hierarchically from the free end to the innermost monomers. Note that Figure III.5 fully reproduces the observation of Ref. [57], where the largest relaxation times could be found near the middle

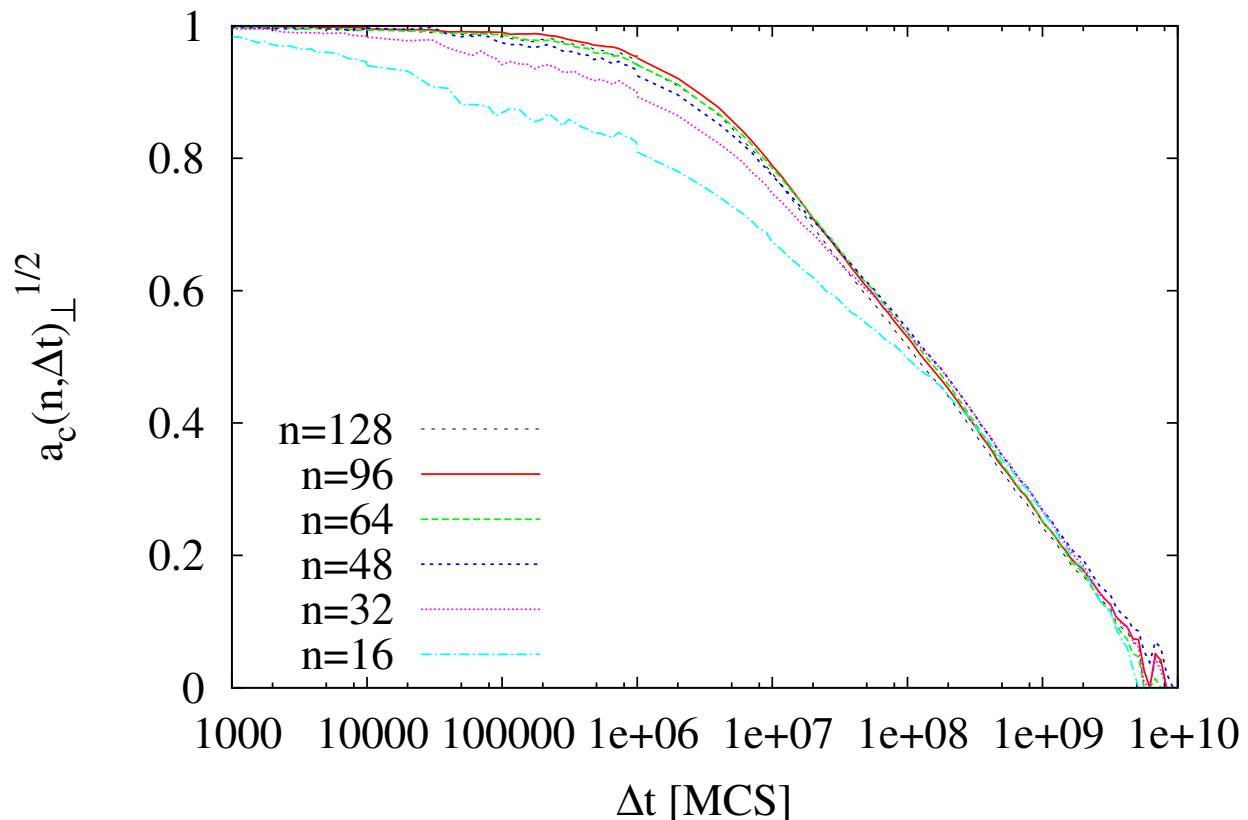


Figure III.6. The square root of the Position vector auto-correlation function $a_c(n, \Delta t)_\perp$ in perpendicular directions for sample #6 indicates the portion of the chain that is not yet relaxed at time Δt .

of the chains: since we show the data of a brush with somewhat larger N/g as discussed by Reith et al. [57], such a behavior is found for a larger level of approximately 0.7 for the correlation function (a smaller portion of Rouse-like relaxation for the more entangled chains of the present study shifts the logarithmic plateaus to higher levels). Furthermore, Figure III.5 shows that even the less suitable, analysis of a decay to $1/e$ can reveal a hierarchical relaxation for the parallel components, if the chains are sufficiently entangled. Nevertheless, such an approach leads always to a systematic underestimation of the terminal relaxation time.

The perpendicular component of the position vector auto-correlation function, which is the dominating contribution for long chains in the brush regime, is shown in Figure III.6. Note that we plot the square root of the correlation function, which we use below

for the determination of the terminal relaxation time. The main difference to the parallel directions is that final relaxation is reached *non-hierarchically*. But in contrast to non-entangled dynamics, relaxation occurs with a *logarithmic time dependence*, showing key signatures of self-similar dynamics *and* retractive motion all the way up to the terminal relaxation. In principle, such a relaxation is only possible, if there is a mechanism that couples the hierarchical relaxation as a function of n in perpendicular direction, while leaving the parallel directions mainly untouched. This is particularly surprising, since the mean square displacement data show that we have to consider the relaxation of chains confined in a tube like environment, and thus, the relaxation of *tube sections* in parallel and perpendicular directions must occur simultaneously. Below, we show by a stepwise generalization of a simple model case that exactly such a hybrid relaxation must follow from what is known about arm retraction dynamics and chain conformations in a brush.

Let us first consider an ideal polymer chain that is stretched by a self-consistent potential that models the interactions with other chains in a brush. This chain is additionally confined by a perfectly straight solid tube of uniform diameter with orientation perpendicular to the grafting plane. In this case, relaxation in parallel direction is finished at the exploration time of the tube diameter, while the perpendicular direction relaxes at the Rouse time of the non-entangled chain in the brush potential.

Next, let us consider that the straight tube is tilted by an angle θ away from the perpendicular direction and let us re-normalize the brush potential such that the time average monomer positions in the coordinate system of the tilted tube do not change. In this case, we obtain the same relaxation behavior as before up to small geometrical coefficients reflecting the tilted tube geometry. We conclude that a constant average tilt of the tube sections does not impose a qualitatively different relaxation behavior of the chain.

The same result is obtained, if we split the tube into s_{max} straight sections of identical length, which are tilted by the same small angle θ away from the perpendicular axis but rotated individually around this axis. In this case, the parallel components of these tube sections resemble a random walk, while the perpendicular component is a directed walk away from the grafting point. Note further that relaxation is also not modified, if we allow for a fluctuation of the length of these tube sections while keeping θ fixed. The reason for this observation is that in all of the above cases we find the very same value of the brush

potential at the very same coordinate along the axis of the confining tube.

In the next step of generalization, we randomly distort the individual tilt angles of the tube sections such that the average perpendicular coordinate of tube section s in a large ensemble of randomly distorted tubes is not modified. Thus, there is still the same value of the brush potential at the very same ensemble average coordinate of the confining tubes. However, this relation no longer holds when analyzing individual tubes. In consequence, the time average force acting on the monomers (and thus, the time average monomer positions in perpendicular direction) becomes a function of the particular tube conformation.

Let us now replace each kink of these individual tubes with a slip link for confining the fluctuations of the chain. Relaxation of the polymer requires in this case that the free end finds its way back through the particular set of slip links. This modification introduces the exponentially growing relaxation times for deep retractions discussed at the introduction, since now the extra chain conformations outside of the slip-link lead to an entropic penalty for retraction. Note that the brush potential with respect to a particular conformation of such a “tube” is sampled on the much shorter Rouse time of this “stretched” chain such that modifications of sections $s \lesssim s_{max} - (N/N_e)^{1/2}$ are fully communicated all along the chain contour prior to the following relaxation steps.

To proceed, we have to make our simple model more self-consistent. To this end, we consider that deviations from the average monomer positions are driven by thermal agitation. Since the confining tube (i.e. the slip link positions) must follow the same statistics as the polymer conformations, an average orientation fluctuation of section s stores an amount of $\approx kT$ of energy. This energy becomes available for sampling extra conformations (different orientations of tube section $i \geq s$) after the corresponding entanglement has been released. Since these modifications are fully communicated in the retraction regime, each relaxing tube sections leads roughly to the same drift of the average monomer positions in perpendicular direction as a result of the modified time average force acting on the monomers independent of the particular position of s .

Finally, we have to take into account that the brush potential causes extra large fluctuations of monomer positions $\propto n \propto s$ around the average positions in perpendicular direction. Thus, the effect on the drift of average monomer positions due to orientation fluctuations is proportional to the weight fraction s of the not yet relaxed tube sections, which enter

squared in $a_c(n, \Delta t)_\perp$. Thus, $a_c(n, \Delta t)_\perp^{1/2}$ must be $\propto s(t)$ at large times. According to equation (I.12), $s(t)$ decays linearly when plotted on logarithmic time axis. This is what we observe in Figure III.6.

We must explain also, why the drift of the average monomer positions in perpendicular direction is not dominating the relaxation in parallel directions, since relaxation of the different directions is coupled by the curvilinear motion of the chain along the confining tube. Notice that the mean square displacements in perpendicular direction take maximum values of approximately $\approx (cn/N)^2$ with a small coefficient, for instance, $c \approx 0.23H$ for a parabolic brush [38]. Ignoring the effect of tube length fluctuations, the monomers, thus, move less than 1/4 along the tube in parallel directions as a result of the drift in perpendicular direction (since this drift is competing with tube length fluctuations, the actual contribution is smaller). The remaining 3/4 of the tube in parallel directions relax by arm retraction. Thus, the coupling in perpendicular direction enters only as a correction that causes a weak decay of the correlation plateau of innermost monomers in Figure III.5 together with additional modes of constraint release [65], dynamic dilution [66], or tube dilation [67] due to the relaxation of surrounding chains.

Note that we neglected above a possible distribution in the number of entanglements per chain as discussed previously for the stress-relaxation of block co-polymers [68]. This is motivated from the fact even for that small N/N_e of the present study we do not observe a dramatic decay of the correlation plateau at intermediate times (see above). Furthermore, this distribution is expected to be of Poisson type and thus, vanishes for $N/N_e \gg 1$ with the same dependence as tube length fluctuations.

Therefore, in order to determine the relaxation time of an entangled brush, we simply fit all data with $a_c(n, \Delta t)_\perp^{1/2} < 1/4$ using functions of the form $\alpha_n \log(\tau_n/\Delta t)$. Here, α_n is the slope of the decay and τ_n the terminal relaxation time of $a_c(n, \Delta t)$. The relaxation time τ of each brush is defined as the average τ_n obtained by this procedure and is reported in Table II. Note that for all samples, except of the least entangled samples #1 and #5, we observe a rather unique logarithmic terminal decay independent of n at large times similar to the one shown in Figure III.6.

A plot of $a_c(n, \Delta t)_\parallel^{1/2} (n/N)^{1/2}$ (taking into account that only a fraction n/N instead of N monomers contribute to the not yet relaxed tube sections) shows that the terminal relaxation

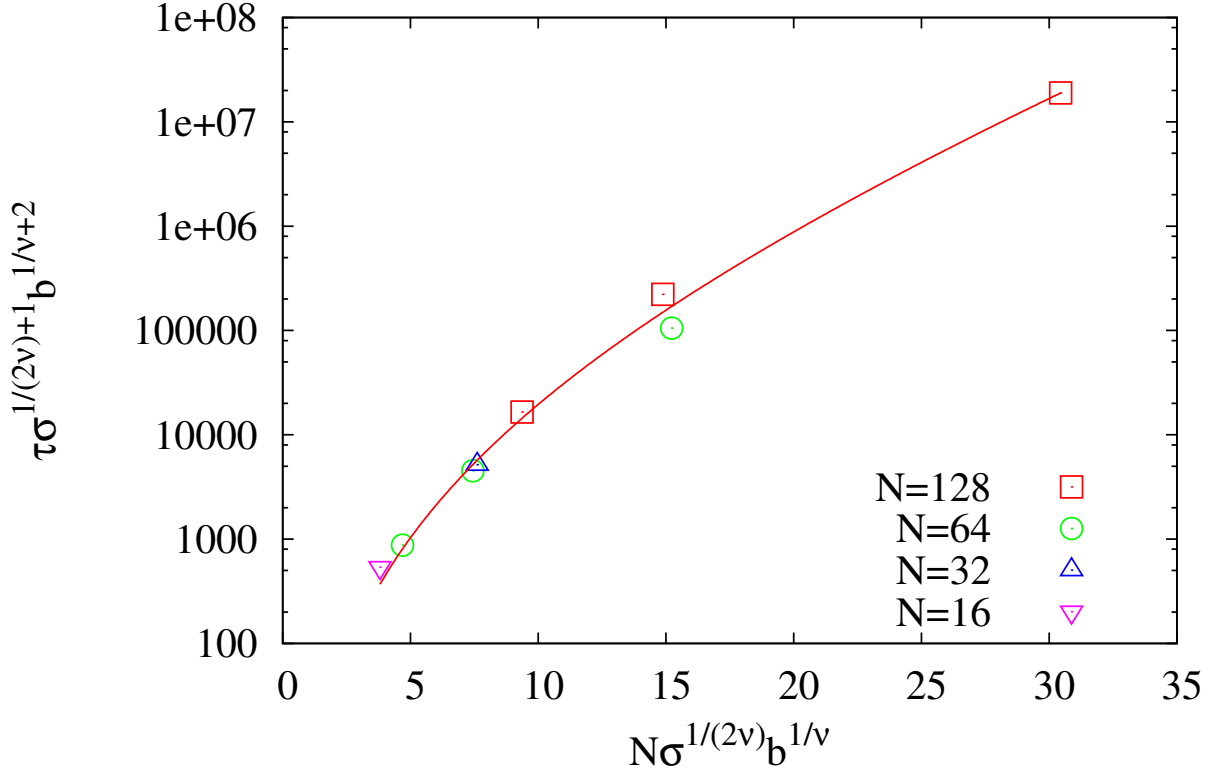


Figure III.7. Dynamic scaling of the terminal relaxation times as a function of the number of blobs $N/g \approx N\sigma^{1/(2\nu)}b^{1/\nu}$ and as multiple of the Rouse time τ_ξ of a blob, $\tau/\tau_\xi \approx \tau\sigma^{1/(2\nu)+1}b^{1/\nu+2}$. The line is a fit to equation (I.9) as described in the text.

in parallel directions occurs simultaneously (see also Figure III.5) for all n somewhat delayed at 2-3 τ , indicating that about 2-3 dives of the full chain are necessary to explore space in parallel directions. Thus, the terminal relaxation times coincide up to a coefficient of order unity, as expected for chains confined in a tube and in contrast to non-entangled dynamics, see equations (I.5) and (I.6) or chains in an array of rods. This observation also rules out that relaxation is driven by a disentanglement in parallel directions (cf. Introduction) for brushes with parameters as in the present study.

The data for terminal relaxation times of Table II are plotted in Figure III.7. We observe a reasonable overlap, if we rescale N by the number of monomers per dynamic blob, $N/g = N\sigma^{1/(2\nu)}b^{1/\nu}$, as determined from monomer mean square displacements and relaxation times using the relation for the Rouse time of a blob, equation (I.4). The data are fit with a

function of form $\tau \propto (N/g)^3 \exp(\beta N/N_e)$ as expected for dense, entangled polymer brushes (cf. equation (I.9)). Since the data are plotted as function of N/g , we can estimate from the coefficient $\beta \approx 0.17 \pm 0.02$ that $N_e/g \approx 5.9 \pm 0.8$. This value is about half of what has been conjectured for flexible polymers in melts [69, 70]. The mean square displacement data in the previous section also indicated that the degree of polymerization between consecutive “slip links”, N_p , is $\approx g$. Thus, we obtain $N_e/N_p \approx 6$, which is clearly larger as what is typically considered in melts or networks with estimates ranging from 2 in Ref. [71] over $7/4$ for the slip tube model [72] to $5/4$ in Ref. [44], for instance. Note further that with $N/g \approx 30$ for sample #6, we obtain $N/N_e \approx 5 \pm 1$. Finally, we want to emphasize that a smaller $N_e/g \approx 6$ for a larger overlap number $P \propto (N/g)$ in brushes as compared to a melt of blobs with $P \propto (N/g)^{1/2}$ is not surprising, if entanglement can be considered as a consequence of polymer overlap. Some part of the qualitative changes (smaller N_e/g and larger N_e/N_p) also might be explained by the over-stretched conformations inside the tube, which causes fewer contacts of higher energy with only some of the overlapping chains.

C. Hierarchical relaxation as analyzed via bond auto-correlation functions

For a local analysis of hierarchical relaxation we use the bond auto-correlation functions $b_c(n, \Delta t)$ defined in equation (III.1). Below, we focus only on the parallel directions in order to minimize the perturbing effect of the coupling in perpendicular direction. For times below the blob relaxation time, equation (I.4), each blob relaxes as part of a swollen Rouse chain to a correlation level of $\xi^2/(b^2g^2) \approx g^{2\nu-2}$. Since this occurs on the relaxation time $\propto (t/\tau_0)^{1+2\nu}$ of a swollen Rouse chain, we expect the bond correlation function $b_c(n, \Delta t)$ to decay as

$$b_c(n, \Delta t) \propto \left(\frac{\Delta t}{\tau_0}\right)^{-(2-2\nu)/(1+2\nu)} \propto \Delta t^{-0.38}. \quad (\text{III.11})$$

Since the inner chain monomers reside in “over-stretched” tubes, we expect beyond τ_ξ and before the Rouse time

$$\tau_n \approx \tau_\xi \left(\frac{n}{g}\right)^2 \quad (\text{III.12})$$

of a section of n monomers, $\Delta t < \tau_n$, a regime with

$$b_c(n, \Delta t)_\parallel \propto \left(\frac{\Delta t}{\tau_e}\right)^{-1/4}, \quad (\text{III.13})$$

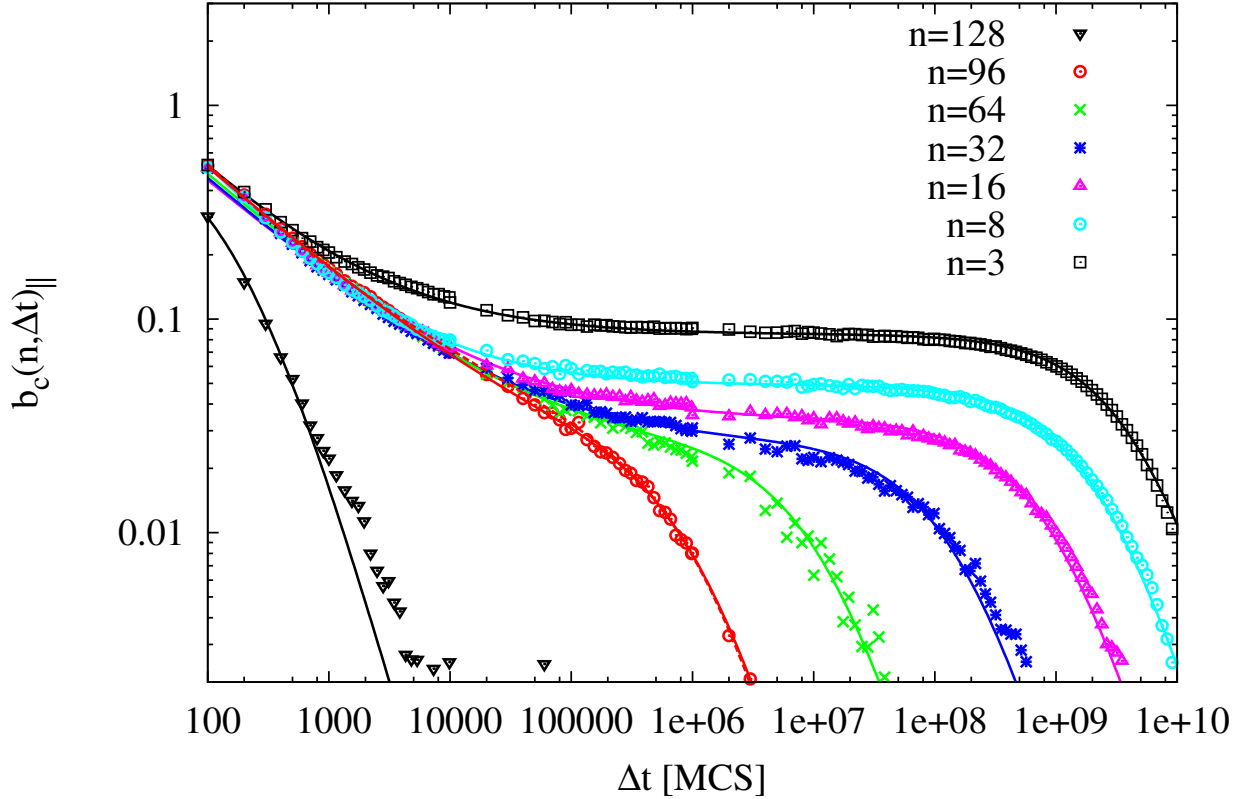


Figure III.8. Bond auto-correlation function in parallel directions for sample #6. The continuous lines are fits to the data as discussed in the text.

similar to entangled chain sections in melt. This regime is followed by an almost constant entanglement plateau (as a function of time) below the terminal relaxation time of a bond, τ_b , that might be affected by tube dilation or constraint release [65–67] or the drift along the tube as function of the relaxing tube sections. The terminal time can be estimated by the retraction time of the chain end along a path of length proportional to the distance to the free end. Assuming a retraction path length $\propto (N - n)$ at constant blob size in perpendicular direction, for simplicity, we obtain

$$\tau_b(n) \approx N(N - n)^2 / g^3 \exp\left(\frac{(N - n)^2}{NN_e}\right) \quad (\text{III.14})$$

using the estimate of Witten et al. [40] and replacing Ng by NN_e in the exponential argument, as above. Note that this entanglement plateau is only possible if $\tau_n < \tau_b(n)$.

Figure III.8 shows a well pronounced plateau for the innermost monomers (small n).

However, the small values of n/N_e , N_e/g , and g that are possible for $n < N \leq 128$ (if there is a significant number of entangled sections $N/N_e \gg 1$ and ignoring the effect of tension blobs smaller than tube diameter) do not allow for an unambiguous observation of the early power law regimes. For instance, an apparent regime with $b_c(n, \Delta t) \propto \Delta t^{-1/4}$ over about one decade in time may also be caused by a power law decay followed by a short plateau. To demonstrate this point we include two different fits for the data of $n = 96$ of the most entangled sample #6. The first fit function reads

$$f_1(t) = (c_1 t^{-0.38} + c_2 t^{-1/4}) (\tau_b / (t + \tau_b))^2, \quad (\text{III.15})$$

while we used

$$f_2(t) = (c_1 t^{-x} + c_2) (\tau_b / (t + \tau_b))^2, \quad (\text{III.16})$$

with a variable $1/4 \leq x \leq 0.38$ in second place. Both functions lead to equally well fits of the data for n roughly in the range of 96 ± 12 , see $n = 96$ in Figure III.8 as example. However, the terminal times τ_b obtained can differ up to a factor of two. Notice that $f_2(t)$ fits clearly better for $n < 84$, while $f_1(t)$ was used for $n > 108$ with an essentially vanishing second power law for $n \rightarrow N$ and that we use a square cut-off $(\tau_b / (t + \tau_b))^2$ to determine τ_b for all monomers $n < N$.

Figure III.9 shows the fit results for $\tau_b(n)$, whereby we interpolate linearly between the results for $f_1(t)$ and $f_2(t)$ in the range $84 < n < 108$ in order to obtain a smooth transition between the domains where both fit functions were used. The difficulty to consistently fit the τ_b data in this transition zone is also visible by the larger scatter of the data for $20 \leq N - n \leq 44$. Nevertheless, the data at all $N - n$ fit well to equation (III.14), while only the small $N - n$ range near the end can be approximated by relaxation times $\propto (N - n)^2$ as one expects from the Rouse model in parallel direction. Note that we exclude the regions with $N - n > 120$ and $N - n < 10$ from the first fit in order to reduce end effects and that the second fit is applied for $N - n < 20$. From the fit to equation (III.14) we obtain $N_e \approx 20 \pm 1$, which gives $N/N_e \approx 6.4 \pm 0.3$ for sample #6, which is in fair agreement with our previous estimate of $N/N_e \approx 5 \pm 1$ from Figure III.7. Note that a similar agreement with larger error bars for N_e is found for the less entangled samples of our study.

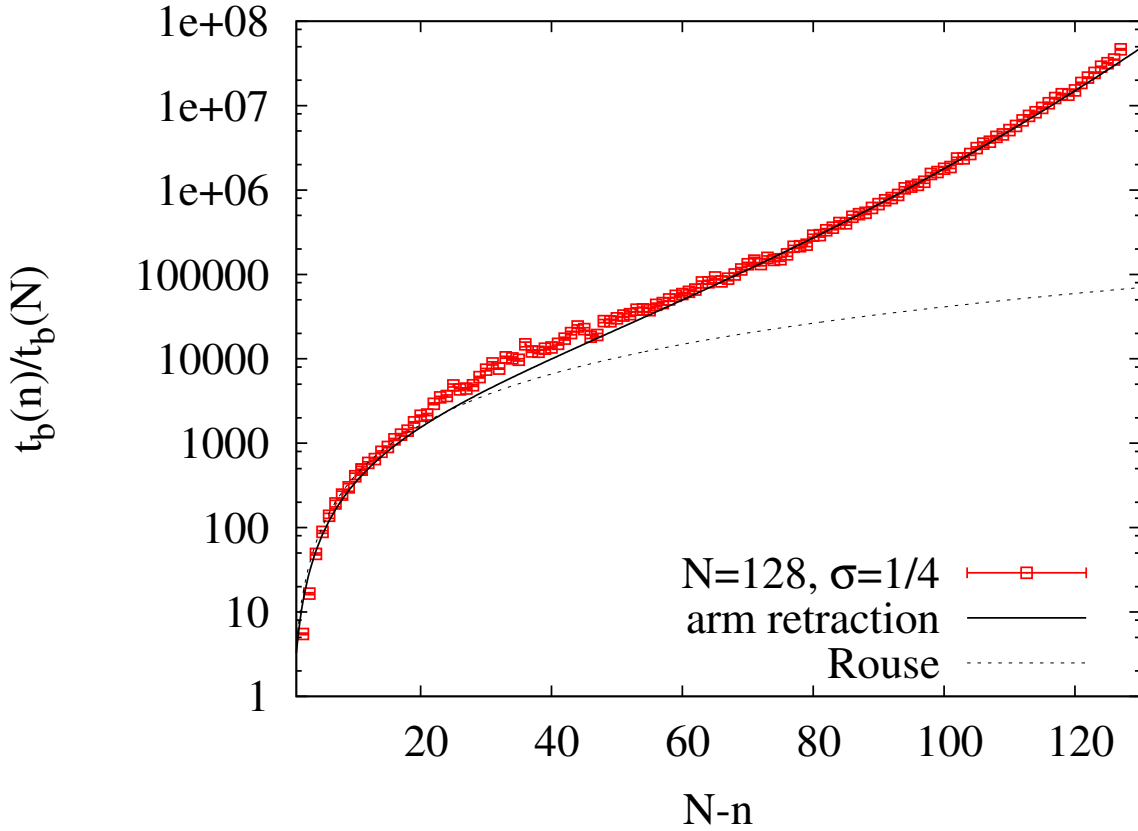


Figure III.9. Terminal bond relaxation times $\tau_b(n)$ in perpendicular direction as estimated from fitting equations (III.15) and (III.16) to the data of sample #6 with $N = 128$ and $\sigma = 1/4$, see text for details. The continuous line (arm retraction) is a fit to equation (III.14), while the dashed line is a fit according to $(N - n)^2$ for small $N - n$.

IV. SUMMARY

In this work, we analyzed in detail the relaxation of monodisperse brushes. We demonstrated for the first time by computer simulations that the relaxation of a polymer brush is governed by retraction dynamics - even for the small number of correlation volumes per chain of the present study. We have shown that this result can be missed with the conventional analysis of the decay of the position vector auto-correlation functions to a level of $1/e$. Such an analysis is suitable for self-similar relaxation, but leads to significant errors in case of arm retraction, since the logarithmic decay at very long times is not fully detected.

The terminal relaxation times of all brushes collapse on a master curve, when time is

rescaled by the relaxation time of a concentration blob, while N and the entanglement degree of polymerization, N_e , are rescaled by the numbers of monomer per concentration blob, g . For the relaxation times of all samples we find an exponential increase $\tau \propto (N/g)^3 \exp(N/N_e)$ as a function of the degree of polymerization, N . From the master plot we obtain $N_e/g \approx 5.9 \pm 0.8$ and (for the most entangled sample of our study) $N/N_e \approx 5 \pm 1$. Thus, entanglement effects already dominate the long time dynamics of a polymer brush much earlier as estimated previously [38] or as compared to monodisperse melt or network data of the same simulation model [45]. This earlier onset of entanglement effects may have several reasons. For instance, the overlap number grows $\propto N$ in a brush as compared to $\propto N^{1/2}$ in a melt, reptation is impossible for grafted chains, and the hierarchical relaxation in combination with the average chain orientation largely reduces the impact of constraint release to surrounding polymers (overlapping chain sections essentially relax at the same time scale). According to our data, entanglements must be considered for $N/g \gtrsim 10$, which is roughly the same criterion as it is used for the application of the strong stretching approximation for chain conformations [34].

The bond auto-correlation functions in parallel directions show a strictly hierarchical relaxation that appears to be not significantly perturbed by the brush potential. Therefore, we conclude that the brush potential does not play an essential role for the relaxation of the chains as postulated previously [41]. However, the position vector auto-correlation data in direction perpendicular to the grafting plane show a collective decay in contrast to the hierarchical relaxation in parallel directions. This qualitatively different behavior can be explained by the predominant orientation of the tube in perpendicular direction which suppresses large scale reorientation of tube sections, such that only fluctuations around an average orientation survive. The brush potential turns the relaxation of these tube orientation fluctuations into a time depending net pulling force acting on the chains, which causes a collective motion of the chain monomers in perpendicular direction after each relaxation step. These collective modes are the dominating contribution in perpendicular direction beyond the Rouse time of the chains, while the exponentially rare contribution of deep retractions can be ignored. In parallel direction, however, these collective modes enter only as a small correction to the classical arm retraction dynamics.

At this point, we also would like to stress that hydrodynamic effects are not accessible with our simulation method. Certainly, hydrodynamics plays a significant role near the free

end and may enhance the collective motion of larger sections of a brush. However, arm retraction is the process of changing the relative positions of two entangled strands, which is difficult to achieve by a collective motion of the chains. Furthermore, the grafting of the polymers damps out collective motion inside the brush. Therefore, we do not expect a significant impact of hydrodynamics for the scaling of the terminal relaxation time as a function of N .

The results of the present work can be applied in further research to understand the dynamics of e.g. bidisperse or polydisperse layers of grafted chains. Polydispersity is most relevant for technical applications, while bidisperse layers are often found in biological systems, for instance, the brush made of MUC1 and MUC4 in the periciliary layer [73].

V. ACKNOWLEDGMENTS

The authors thank the ZIH Dresden for a generous grant of computing time, the DFG for funding projects LA 2735/2-1 and KR 2854/3-1, and M. Hoffmann for providing the numerical solution of grafted Rouse chains. T.C.B. McLeish, M. Rubinstein, H. Merlitz, and J.-U. Sommer are thankfully acknowledged for helpful discussions.

-
- [1] V. Torchilin, “Targeted pharmaceutical nanocarriers for cancer therapy and imaging” *AAPS J.* **9**, E128 (2007).
 - [2] D. Napper, “Polymeric Stabilisation of Colloidal Dispersions”, Academic Press, London, United Kingdom (1983).
 - [3] W. Russel, D. Saville, and W. Schowalter, “Colloidal Dispersions”, Cambridge University Press, Cambridge, United Kingdom (1989).
 - [4] J. Klein, E. Kumacheva, D. Mahalu, D. Perahia, and L. Fetters, “Reduction of frictional forces between solid surfaces bearing polymer brushes”, *Nature* **370**, 634 (1994).
 - [5] J. Klein, D. Perahia, and S. Warburg, “Forces between polymer-bearing surfaces undergoing shear”, *Nature* **352**, 143 (1991).
 - [6] T. Moro, Y. Takatori, K. Ishihara, T. Konno, Y. Takigawa, T. Matsushita, U.-I. Chung, K. Nakamura, and H. Kawaguchi, “Surface grafting of artificial joints with a biocompatible polymer

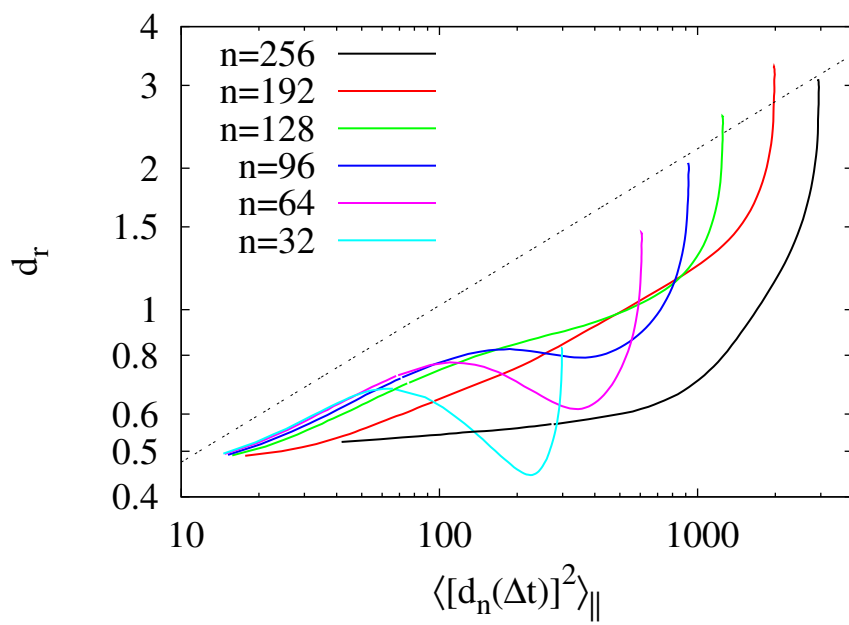
- for preventing periprosthetic osteolysis”, *Nature Mater.* **3**, 829 (2004).
- [7] A. Galuschko, L. Spirin, T. Kreer, A. Johner, C. Pastorino, J. Wittmer, and J. Baschnagel, “Frictional Forces between Strongly Compressed, Nonentangled Polymer Brushes: Molecular Dynamics Simulations and Scaling Theory”, *Langmuir* **26**, 6418 (2010).
- [8] L. Spirin, A. Galuschko, T. Kreer, A. Johner, J. Baschnagel, and K. Binder, “Polymer-brush lubrication in the limit of strong compression”, *Eur. Phys. J. E* **33**, 307 (2010).
- [9] P. Uhlmann, H. Merlitz, J.-U. Sommer, and M. Stamm, “Polymer brushes for surface tuning”, *Macromol. Rapid Commun.* **30**, 732 (2009).
- [10] W. Cui, C.-X. Wu, H. Merlitz, J.-U. Sommer, “Numerical evidences for a free energy barrier in starlike polymer brushes”, *J. Chem. Phys.* **139**, 134910 (2013).
- [11] S.-Z. He, H. Merlitz, C.-F. Su, and C.-X. Wu, “Static and dynamic properties of grafted ring polymer: molecular dynamics simulation” *Chinese Physics B*, **22** 016101 (2013).
- [12] W. Cui, C.-F. Su, H. Merlitz, C.-X. Wu, and J.-U. Sommer, “Structure of dendrimer brushes: Mean-field theory and MD simulations”, *Macromolecules* **47**, 3645 (2014).
- [13] M. Hoffmann, M. Lang, J.-U. Sommer, “Gelation threshold of cross-linked polymer brushes”, *Phys. Rev. E* **83**, 021803 (2011).
- [14] M. Lang, M. Hoffmann, R. Dockhorn, M. Werner, J.-U. Sommer, “Fluctuation driven height reduction of crosslinked polymer brushes: A Monte Carlo study”, *J. Chem. Phys.* **139**, 164903 (2013).
- [15] L. Spirin, A. Galuschko, T. Kreer, K. Binder, J. Baschnagel, “Polymer-brush lubricated surfaces with colloidal inclusions under shear inversion”, *Phys. Rev. Lett.* **106**, 168301 (2011).
- [16] H. Merlitz, C.-X. Wu, and J.-U. Sommer, “Inclusion free energy of nanoparticles in polymer brushes”, *Macromolecules* **45** 8494 (2012).
- [17] T. Kreer, “Polymer-brush lubrication: A review of recent theoretical advances”, *Soft Matter* (2016), article in press, DOI: 10.1039/c5sm02919h.
- [18] J. Klein, “Repair or Replacement - A Joint Perspective”, *Science* **323**, 47 (2009).
- [19] B. Zdyrko, V. Klep, X. Li, Q. Kang, S. Minko, X. Wen, and I. Luzinov, “Polymer brushes as active nanolayers for tunable bacteria adhesion”, *Mater. Sci. Eng. C* **29**, 680 (2009).
- [20] A. G. Goicochea, E. Mayoral, J. Klapp, C. Pastorino, “Nanotribology of biopolymer brushes in aqueous solution using dissipative particle dynamics simulations: an application to PEG

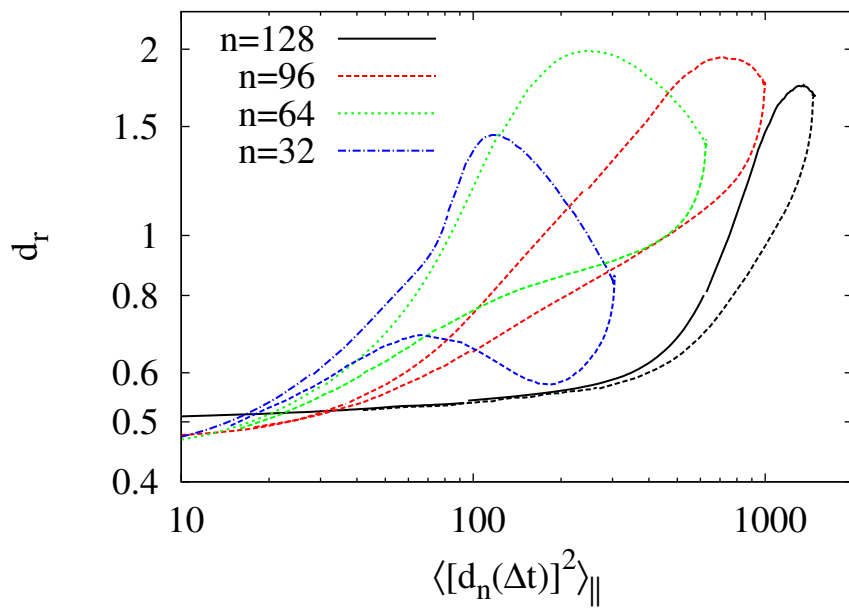
- covered liposomes in a theta solvent” *Soft Matter*, **10**, 166 (2014).
- [21] R. C. Advincula, W. J. Brittain, K. C. Caster, J. Ruehe (eds.), “Polymer Brushes”, Wiley-VCH, Weinheim, (2004).
- [22] I.V. Neratova, T. Kreer, J.-U. Sommer, “Translocation of Molecules with Different Architectures through a Brush-Covered Microchannel”, *Macromolecules*, **48**, 3756 (2015).
- [23] K. Binder, T. Kreer, A. Milchev, “Polymer brushes under flow and in other out-of-equilibrium conditions”, *Soft Matter* **7**, 7159 (2011).
- [24] L. Spirin, T. Kreer, “Strongly compressed polyelectrolyte brushes under shear” *ACS Macro Letters* **2**, 63 (2013).
- [25] T. Kreer, S. M. Balko, “Scaling theory for compressed polymer-brush bilayers”, *ACS Macro Letters* **2**, 944 (2013).
- [26] S. M. Balko, T. Kreer, D. J. Mulder, P. J. Costanzo, T. E. Patten, T. L. Kuhl, “Using Thiol–Gold Bond Formation To Bridge Surfaces with a Polymer Brush: SFA Experiments and MD Simulations”, *Macromolecules*, **46**, 9826 (2013).
- [27] A. N. Semenov, “Contribution to the theory of microphase layering in block-copolymer melts”, *Zh. Eksp. Teor. Fiz.* **88**, 1242 (1985).
- [28] S. T. Milner, T. A. Witten, M. E. Cates, “A Parabolic Density Profile for Grafted Polymers”, *Europhys. Lett.* **5**, 413 (1988).
- [29] A. Skvortsov, I. Pavlushkov, A. Gorbunov, Y. Zhulina, O. Borisov, and V. Pryamitsyn, “Structure of densely grafted polymeric monolayers”, *Vysokomol. Soedin., Ser. A* **30**, 1598 (1988).
- [30] V. M. Amoskov, V. A. Priamitsyn, “Theory of Monolayers of Non-Gaussian Polymer Chains grafted onto a Surface” *J. Chem. Soc. Faraday Trans.* **90**, 889 (1994).
- [31] R. R. Netz, M. Schick, “Classical theory of polymer brushes”, *Europhys. Lett.* **38**, 37 (1997).
- [32] S. Alexander, “Adsorption of chain molecules with a polar head a scaling description”, *J. Phys. France* **38**, 983 (1977).
- [33] P. G. de Gennes, “Conformations of Polymers Attached to an Interface”, *Macromolecules* **13**, 1069 (1980).
- [34] D. Romeis, M. Lang, “Excluded volume effects in polymer brushes at moderate chain stretching”, *J. Chem. Phys.* **141**, 104902 (2014).

- [35] J. C. Le Guillou, J. Zinn-Justin, “Critical exponents for the n-vector model in three dimensions from field theory” *Phys. Rev. Lett.* **39**, 95-98 (1977).
- [36] G. A. Baker, B. G. Nickel, D. I. Meiron, “Critical indices from perturbation analysis of the Callan-Symanzik equation”, *Phys. Rev. B* **17**, 1365 (1978).
- [37] M. Rubinstein, R. H. Colby, “Polymer Physics”, Oxford University Press, Oxford (2003).
- [38] L. I. Klushin, A. M. Skvortsov, “Critical Dynamics of a Polymer Chain in a Grafted Monolayer”, *Macromolecules* **24**, 1549 (1991).
- [39] A. Johner, J. F. Joanny, “Dynamics of polymeric brushes: End exchange and bridging kinetics”, *J. Chem. Phys.* **98**, 1647 (1993).
- [40] T. Witten, L. Leibler, P. Pincus, “Stress Relaxation in the Lamellar Copolymer Mesophase”, *Macromolecules* **23**, 824 (1990).
- [41] K. P. O’Connor, T. C. B. McLeish, “‘Molecular Velcro’: Dynamics of a Constrained Chain into an Elastomer Network”, *Macromolecules* **26** (1993) 7322-7325.
- [42] K. P. O’Connor, T. C. B. McLeish, “Entangled Dynamics of Healing End-grafted Chains at a Solid/Polymer Interface”, *Faraday Discuss.* **98** (1994) 67-78.
- [43] Note that there is a numerical coefficient connecting the entanglement degree of polymerization and tube diameter as discussed in [44, 45].
- [44] R. G. Larson, T. Sridhar, L. G. Leal, G. H. McKinley, A. E. Likhtman, T. C. B. McLeish, “Definitions of entanglement spacing and time constants in the tube model”, *J. Rheol.* **47**, 809 (2003).
- [45] M. Lang, “Monomer Fluctuations and the Distribution of Residual Bond Orientations in Polymer Networks”, *Macromolecules* **46**, 9782 (2013).
- [46] L. Bureau, L. Leger, “Sliding Friction at a Rubber/Brush Interface”, *Langmuir* **20** (2004) 4523-4529.
- [47] M. Geoghegan, C. J. Clarke, F. Boue, A. Menelle, T. Russ, D. G. Bucknall, “The Kinetics of Penetration of Grafted Polymers into a Network”, *Macromolecules* **32** (1999) 5106-5114.
- [48] C. J. Clarke, “The kinetics of polymer brush penetration into a high molecular weight matrix”, *Polymer* **37**, (1996) 4747-4752.
- [49] A. Chenneviere, E. Drockenmuller, D. Damiron, F. Cousin, F. Boue, F. Restagno, L. Leger, “Quantitative Analysis of interdigitation Kinetics between a Polymer Melt and a Polymer

- Brush”, *Macromolecules* **46** (2013) 6955-6962.
- [50] M. Murat and G. Grest, “Structure of a Grafted Polymer Brush: A Molecular Dynamics Simulation” *Macromolecules* **22**, 4054 (1989).
- [51] P.-Y. Lai and K. Binder, “Structure and dynamics of grafted polymer layers: A Monte Carlo simulation” *J. Chem. Phys.* **95**, 9288 (1991).
- [52] P.-Y. Lai and K. Binder, “Structure and dynamics of polymer brushes near the Θ -point: A Monte Carlo simulation”, *J. Chem. Phys.* **97** 586 (1992).
- [53] J. F. Marko, A. Chakrabarti, “Static and dynamic collective correlations of polymer brushes”, *Phys. Rev. E* **48**, 2739 (1993).
- [54] K. Binder, P.-Y. Lai, J. Wittmer, “ Monte Carlo Simulations of Chain Dynamics in Polymer Brushes”, *Faraday Discuss.* **98**, 97 (1994).
- [55] G. Grest, “Grafted polymer brushes in polymeric matrices”, *J. Chem. Phys.* **105** (1996) 5532-5541.
- [56] G. He, H. Merlitz, J. Sommer, and C. Wu, “Static and Dynamic Properties of Polymer Brushes at Moderate and High Grafting Densities: A Molecular Dynamics Study”, *Macromolecules* **40**, 6721 (2007).
- [57] D. Reith, A. Milchev, P. Virnau, K. Binder, “Computer Simulation Studies of Chain Dynamics in Polymer Brushes ” *Macromolecules* **45**, 4381 (2012).
- [58] T. Kreer, H. H. Müser, “On the tribology and rheology of polymer brushes in good solvent conditions: a molecular dynamics study”, *Wear* **254** (2003) 827-831.
- [59] F. L. Verso, L. Yelash, K. Binder, “Dynamics of Macromolecules Grafted in Spherical Brushes under Good Solvent Conditions”, *Macromolecules* **46** (2013) 4716-4722.
- [60] I. Carmesin, K. Kremer, “The Bond Fluctuation Method: A New Effective Algorithm for the Dynamics of Polymers in All Spatial Dimensions”, *Macromolecules* **21**, 2819 (1988).
- [61] H. P. Deutsch, K. Binder, “Interdiffusion and self-diffusion in polymer mixtures: A Monte Carlo Study”, *J. Chem. Phys.* **94**, 2294-2304 (1991).
- [62] S. Nedelcu, M. Werner, M. Lang, J.-U. Sommer, “GPU Implementations of the Bond Fluctuation Model”, *J. Comp. Phys.* **231**, 2811 (2012).
- [63] M. Hoffmann, “Theory and Simulation of cross-linked Polymers at Surfaces”, Diploma thesis, Dresden (2009).

- [64] For instance, if $\langle [d_n(\Delta t)]^2 \rangle_{\perp} \propto t^x$ while $\langle [d_n(\Delta t)]^2 \rangle_{\parallel} \propto t^y$, we obtain $d_r \propto \langle [d_n(\Delta t)]^2 \rangle_{\parallel}^{x/y-1}$.
- [65] J. L. Viovy, M. Rubinstein, R. H. Colby, "Constraint Release in Polymer Melts: Tube Reorganization versus Tube Dilution", *Macromolecules* **24** (1991) 3587-3596.
- [66] R. C. Ball, T. C. B. McLeish, "Dynamic Dilution and the Viscosity of Star Polymer Melts", *Macromolecules* **22** (1989) 1911-1913.
- [67] G. Marucci, "Relaxation by Reptation and Tube Enlargement: A Model for Polydisperse Polymers", *J. Pol. Sci B.* **23** (1985) 159-177.
- [68] M. Rubinstein, S. P. Obukhov, "Power-Law-Like Stress Relaxation of Block Copolymers: Disentanglement Regimes", *Macromolecules* **26** (1993) 1740-1750.
- [69] Y.-H. Lin, "Number of Entanglement Strands per Cubed Tube Diameter, a Fundamental Aspect of Topological Universality in Polymer Viscoelasticity", *Macromolecules* **20**, 3080 (1987).
- [70] T. A. Kavassalis, J. Noolandi, "New View of Entanglements in Dense Polymer Systems", *Phys. Rev. Lett.* **59**, 2674 (1987).
- [71] R. Everaers, "Topological versus rheological entanglement length in primitive-path analysis protocols, tube models, and slip-link models" *Phys. Rev. E* **86**, 022801 (2012).
- [72] M. Rubinstein, S. Panyukov, "Elasticity of Polymer Networks", *Macromolecules* **35**, 6670 (2002).
- [73] B. Button, L.-H. Cai, C. Ehre, M. Kesimer, D.B. Hill, J. K. Sheehan, R. C. Boucher, M. Rubinstein, "A periciliary brush promotes the lung health by separating the mucus layer from airway epithelia", *Science* **337** (2012) 937-941.





This figure "TOC.jpg" is available in "jpg" format from:

<http://arxiv.org/ps/2104.05264v1>